Altered Hippocampal Glutamatergic Neurotransmission and Cognitive Impairment in APP Knock-In Mice

C.A. Findley[1, 2], S.A. McFadden[1], T. Hill[1], M.R. Peck[1], K. Quinn[1], K.N. Hascup[1, 2, 3], E.R. Hascup[1, 2*]

[1]Neuroscience Institute, Dale and Deborah Smith Center for Alzheimer's Research and Treatment, Depts of Neurology, [2]Pharmacology, and [3]Medical Microbiology, Immunology and Cell Biology, Southern Illinois University School of Medicine, Springfield, IL, USA

*Erin R. Hascup, Department of Neurology, Dale and Deborah Smith Center for Alzheimer's Research and Treatment, Southern Illinois University School of Medicine, P.O. Box 19628, Springfield, IL 62794-9628, USA. Email: ehascup@siumed.edu

Potential Keywords: cognition, amyloid, learning, memory, sex differences, Alzheimer's disease

Running head: Glutamate and cognition in $APP^{NL\text{-}F/NL\text{-}F}$ mice

Abbreviations: Alzheimer's disease (AD), morris water maze (MWM), novel object recognition (NOR), dentate gyrus (DG), amyloid-beta (Aβ), microelectrode array (MEA), platinum (Pt), glutamate oxidase (GluOX), 1,3 phenylenediamine dihydrochloride (mPD), standard error of the mean (SEM), time to 80% signal decay (T_{80})

Data Availability: The data to support the findings of this study are available from the corresponding author upon reasonable request.

Funding: This work was supported by the National Institutes of Health [R01 AG057767, R01 AG061937], the Dale and Deborah Smith Center for Alzheimer's Research and Treatment, and the Kenneth Stark Endowment.

Conflict of Interest: The authors have no conflicts of interest to disclose.

Ethics Approval: Protocols for animal use were approved by the *Institutional Animal Care and Use Committee* at Southern Illinois University School of Medicine (Protocol #2022-055).

Abstract

It is well established that glutamatergic neurotransmission plays an essential role in learning and memory. Previous studies indicate that glutamate dynamics shift with Alzheimer's disease (AD) progression, contributing to negative cognitive outcomes. In this study, we characterized hippocampal glutamatergic signaling with age and disease progression in a knock-in mouse model of AD ($APP^{NL\text{-}F/NL\text{-}F}$). At 2-4 and 18+ months old, male and female $APP^{NL/NL}$, $APP^{NL\text{-}F/NL\text{-}F}$, and C57BL/6 mice underwent cognitive assessment using Morris water maze (MWM) and Novel Object Recognition (NOR). Then, basal and 70 mM KCl stimulus-evoked glutamate release was measured in the dentate gyrus (DG), CA3, and CA1 regions of the hippocampus using a glutamate-selective microelectrode in anesthetized mice. Glutamate recordings support elevated stimulus-evoked glutamate release in the DG and CA3 of young $APP^{NL\text{-}F/NL\text{-}F}$ male mice that declined with age compared to age-matched control mice. Young female $APP^{NL\text{-}F/NL\text{-}F}$ mice exhibited increased glutamate clearance in the CA1 that slowed with age compared to age-matched control mice. Male and female $APP^{NL\text{-}F/NL\text{-}F}$ mice exhibited decreased CA1 basal glutamate levels, while males also showed depletion in the CA3. Cognitive assessment demonstrated impaired spatial cognition in aged male and female $APP^{NL\text{-}F/NL\text{-}F}$ mice, but only aged females displayed recognition memory deficits compared to age-matched control mice. These findings confirm a sex-dependent hyper-to-hypoactivation glutamatergic paradigm in $APP^{NL\text{-}F/NL\text{-}F}$ mice. Further, data illustrate a sexually dimorphic biological aging process resulting in a more severe cognitive phenotype for female $APP^{NL\text{-}F/NL\text{-}F}$ mice than their male counterparts. Research

55 outcomes mirror that of human AD pathology and provide further evidence of divergent

56 AD pathogenesis between sexes.

57

Introduction

Glutamate is the most abundant neurotransmitter in the brain, expressed by the vast majority of excitatory neurons (Purves D *et al.* 2001). It is a central component of many neurological functions, including learning and memory (McEntee and Crook 1993). Glutamate dynamics are impacted by aging-related cortical thinning and synaptic pruning that occurs in the hippocampus and prefrontal cortex, amongst other areas (Segovia *et al.* 2001; Cox *et al.* 2022). Aging diminishes glutamate levels over time, impacting pivotal processes for learning and memory and contributing to cognitive decline commonly associated with age (Cox *et al.* 2022; Gasiorowska *et al.* 2021; Segovia *et al.* 2001).

Many pathological conditions involve dysregulation of the glutamatergic system, including epilepsy and aging-related neurodegenerative disorders like Alzheimer's disease (AD). These conditions include loss of glutamatergic homeostasis that results in neuronal death and brain atrophy (Lewerenz and Maher 2015a). Glutamatergic hyperactivity has been characterized in both AD mouse models and human pathology, first appearing before the onset of plaque deposition and cognitive symptomology. Prior work from our laboratory demonstrated a hippocampal glutamatergic imbalance that appears in young (2-6 months old) male AβPP/PS1 transgenic AD mice, and shifts in a temporal-specific manner with disease progression (Hascup *et al.* 2020). The CA1 and dentate gyrus (DG) subregions displayed glutamatergic hyperactivity that continued into later disease stages, with a significant drop-off around 18 months of age in the CA1. The pattern found in the CA1 reflects the hyper-to-hypoactivation hypothesis, describing early overstimulation of glutamatergic receptors and astrocytic glutamate transporters

leading to dyshomeostasis at the glutamatergic synapse in AD pathology (Parsons *et al.* 2007; Findley *et al.* 2019; Olney *et al.* 1997). As well, our laboratory found increased basal glutamate levels in the CA1, CA3, and DG of AβPP/PS1 male mice starting at 6 months of age and continued throughout disease progression. These findings provided further evidence supporting the loss of hippocampal signal-to-noise ratio with disease progression in AD pathology. Signal-to-noise ratio describes the threshold by which neuronal stimulation must overcome to evoke an action potential. An imbalance in this ratio indicates dyshomeostasis at the glutamatergic synapse and can hinder long-term potentiation (Parsons *et al.* 2007; Findley *et al.* 2019).

This study aims to characterize hippocampal glutamate dynamics in a novel knock-in mouse model of AD ($APP^{NL\text{-}F/NL\text{-}F}$). The $APP^{NL\text{-}F/NL\text{-}F}$ mouse model may better recapitulate the human condition and avoids confounding variables associated with transgenic mice, such as overexpression of the amyloid precursor protein and presenilin-1 (Saito *et al.* 2014). $APP^{NL\text{-}F/NL\text{-}F}$ mice have a knock-in APP gene with an endogenous promoter and humanized amyloid-beta (Aβ) sequence. The Aβ sequence used also appears in most human sporadic and familial AD patients (Saito *et al.* 2014). There is no genetic overexpression, however, this model does have the Swedish mutation to APP (NL) that raises total Aβ levels. Presenillin-1 has the Iberian mutation (F), which increases the $Aβ_{42}$: $Aβ_{40}$ ratio. This model typically shows plaque deposition at around 6 months old, with steady plaque accumulation up to 18 months old (Masuda *et al.* 2016; Shah *et al.* 2018; Britz *et al.* 2022).

To our knowledge, glutamatergic neurotransmission throughout disease progression has not previously been characterized in this model. Further, investigation of sex

differences for AD mice is limited (Kundu *et al.* 2021; Britz *et al.* 2022; Masuda *et al.* 2016). Amyloidosis throughout disease progression has been observed as similar between male and female $APP^{NL\text{-}F/NL\text{-}F}$ mice, while reports of cognitive symptomology yield mixed results (Britz *et al.* 2022; Kundu *et al.* 2021). Prior work from our laboratory investigating glutamate dynamics has been limited to male transgenic (AβPP/PS1) mice (Hascup *et al.* 2020). Thus, it remains unclear how sex may impact glutamate and cognition with age and disease progression in this model.

To address this question, we utilized glutamate-specific *in vivo* microelectrode array (MEA) recordings in the hippocampus of $APP^{NL\text{-}F/NL\text{-}F}$ mice at young (2-4 months old) and aged (18+ months old) time points. The $APP^{NL/NL}$ control model that expresses only the APP Swedish mutation was also examined. Comparing results from the $APP^{NL\text{-}F/NL\text{-}F}$ model to the $APP^{NL/NL}$ model allows for the elimination of confounding variables such as non-Aβ fragments of APP, including C-terminal fragments (Saito *et al.* 2014). We hypothesized that $APP^{NL\text{-}F/NL\text{-}F}$ mice would exhibit presymptomatic hippocampal glutamatergic hyperactivation that shifts with age and disease progression.

Materials and Methods

Animals: Founder male and female C57BL/6 (RRID:IMSR JAX:000,664) were obtained from Jackson Laboratory (Bar Harbor, ME). Founder $APP^{NL/NL}$ (RRID:IMSR_RBRC06342) and $APP^{NL\text{-}F/NL\text{-}F}$ (RRID: IMSR_RBRC06343) male and female mice were obtained from Riken (Tokyo, Japan). Founder mice of all strains were used to start breeding colonies of the respective genotypes and their progeny were used for all experiments. Protocols for animal use were approved by the *Institutional Animal Care and Use Committee* at Southern Illinois University School of Medicine,

which is accredited by the Association for Assessment and Accreditation of Laboratory Animal Care. The study was not pre-registered. Mice were group housed according to sex and genotype on a 12:12 h light-dark cycle, and food and water were available *ad libitum*. All experiments were conducted during the light phase. Mouse cages were pseudo-randomized using the Microsoft Excel 2013 randomization function to generate random decimal numbers between 0 and 1 for each mouse cage. No exclusion criteria were pre-determined. 164 animals were used in this study including the following groups: 2-4 months old males (C57BL/6 (n=13), $APP^{NL/NL}$ (n=14), $APP^{NL-F/NL-F}$ (n=16)) and females (C57BL/6 (n=14), $APP^{NL/NL}$ (n=13), $APP^{NL-F/NL-F}$ (n=12)); 18+ months old males (C57BL/6 (n=14), $APP^{NL/NL}$ (n=12), $APP^{NL-F/NL-F}$ (n=15)) and females (C57BL/6 (n=15), $APP^{NL/NL}$ (n=13), $APP^{NL-F/NL-F}$ (n=13). All mice underwent cognitive assessment and *in vivo* glutamate recordings with the exception of electrode failure or death before or during glutamate recordings. Immediately following anesthetized glutamate recordings, mice were euthanized with an overdose of isoflurane followed by rapid decapitation. Genotypes were confirmed by collecting a 5 mm tail tip for analysis by TransnetYX, Inc (Cordova, TN). All mice were tattooed with unique numerical identifiers to blind researchers throughout experimental paradigms.

8-Day Hidden Platform Morris Water Maze (MWM): The MWM examines spatial learning and long-term memory through requiring mice to utilize external visual cues to locate the hidden platform (submerged 1 cm below the opaque water surface), regardless of starting position in the pool. The MWM consists of one acclimation day, five consecutive learning days, and a delayed probe challenge. The five learning days include three trials, up to 90-seconds in duration starting from three different entry

150 points into the pool (order is randomized throughout the learning days) with at least a
151 20-minute inter-trial-interval to test spatial learning capabilities. After two days without
152 testing mice then undergo a probe challenge consisting of one 60-second trial with the
153 platform removed from the pool to test long-term spatial memory recall. The ANY-maze
154 video tracking system (Stoelting, Wood Dale, IL) tracks and analyzes several
155 parameters throughout the learning days and probe challenge, including average
156 speed, cumulative distance from platform, platform entries, latency to first platform
157 entry, and path efficiency to first platform entry.

158 **Novel Object Recognition (NOR)**: NOR is designed to investigate object recognition
159 memory by measuring the exploration time of a novel object compared to a familiar
160 object within a testing arena. One week after the MWM probe challenge, mice were
161 habituated to the NOR testing arena for 30 minutes. Familiarization training occurred
162 24 hours later in which two similar objects are placed into the arena and the mice were
163 allowed to explore for 5 minutes. After a 24-hour inter-session-interval, mice were
164 placed back into the arena for 5 minutes with one familiar object from the previous
165 training day and a novel object to test retention. The ANY-maze video tracking system
166 was utilized to track animals throughout the three experiment days and provides
167 measures of distance traveled, average speed, and exploration time to determine the
168 novel object discrimination index.

169 ***In Vivo* Electrochemistry**: Enzyme-based MEAs with platinum (Pt) recording surfaces
170 were prepared for *in vivo* glutamate measurements and calibrated through the FAST-16
171 recording software as previously described (Hascup and Hascup 2015; Hascup *et al.*
172 2020; Hascup *et al.* 2007). A glutamate oxidase (GluOX) solution was applied to a Pt

recording surface to allow for enzymatic degradation of glutamate to α-ketoglutarate and the electroactive reporter molecule H_2O_2. The adjacent self-referencing recording surface was only coated with an inactive protein matrix and cannot enzymatically generate H_2O_2 from l-glutamate. The FAST-16 system utilizes the self-referencing site for offline subtraction from the GluOX coated site as a localized control mechanism. A potential of + 0.7 V vs an Ag/AgCl reference electrode was applied to the recording sites for oxidation of H_2O_2. Recording sites were then electroplated with 5 mM 1,3 phenylenediamine dihydrochloride (mPD) in 0.05M phosphate buffered saline 72 hours after enzymatic coating. mPD provides an exclusion layer that blocks the detection of possible interferants that are electrochemically active at + 0.7 V. MEA calibration occurred on experiment day, with an average ± standard error of the mean (SEM) glutamate sensitivity of 4.8610 ± 0.0002 pA/μM (R^2 = 0.998 ± 0.001), selectivity ratio of 126 ± 11 to 1, and limit of detection of 0.9305 ± 0.0652 μM based on a signal-to-noise ratio of 3. A micropipette (inner diameter ~20μm) was then waxed on to the MEA (50-100μm from the electrode surface) for local application of 70mM KCl. Mice were placed into a stereotaxic frame under isoflurane anesthesia and a craniotomy was performed for insertion of the MEA assembly into the hippocampus. Body temperature was maintained with a heated recirculating bath pump attached to a water pad. The starting hemisphere and hippocampal subregion was randomized across the CA1 (AP: −2.0, ML: ±1.0, DV: −1.7 mm) or CA3 (AP: −2.0, ML: ±2.0, DV: −2.2 mm)]. After CA1 recordings, the MEA was lowered into the DG (AP: −2.0, ML: ±1.0, DV: −2.2 mm). MEAs were allowed to baseline for 60 minutes after initial insertion before a 10 s basal glutamate determination and pressure ejection studies commenced. An additional 20-

196 minute baseline period occurred between each hippocampal subregion. Pressure
197 ejections involved a constant volume (~100-200nL) of 70mM KCl locally applied using a
198 Picospritzer (Parker Hannafin, Morton, IL) attached to the micropipette to evoke
199 glutamate release.

200 **Cresyl Violet Staining**: Mice were euthanized after stimulation by isoflurane overdose
201 and rapid decapitation with sharp scissors. The brain was extracted and fixed in 4%
202 paraformaldehyde for 48 hours and then transferred to 30% sucrose for storage. A
203 cryostat (Model HM525 NX, Thermo Fisher Scientific) was used to obtain 20-micron
204 coronal sections throughout the hippocampus. Slices were mounted on a glass slide,
205 stained with cresyl violet, and coverslipped to verify MEA placement for each mouse.

206 **Statistical Analysis**: Sample size was determined based on previous MWM and
207 electrochemical data using multiple mouse models. GraphPad Prism 9 Software (La
208 Jolla, CA; RRID:SCR 002798) was used for statistical analyses. Statistical tests are
209 listed in each figure legend. Data were not assessed for normality. A single Grubb's test
210 (alpha = 0.05) was utilized to identify significant outliers in each group. Data are
211 represented as mean ± SEM and statistical significance was defined as $p < 0.05$.

212 **Results**

213 **Alterations to glutamatergic neurotransmission before cognitive symptoms in**
214 **young AD mice**

215 At 2-4 months of age, $APP^{NL/NL}$, $APP^{NL\text{-}F/NL\text{-}F}$, and C57BL/6 mice underwent a cognitive
216 battery to assess spatial navigation and retention memory. As expected, no significant
217 genotype differences were observed for either sex in spatial learning and memory

(Supplementary Figure 1A-E). During the NOR retention day, male mice showed no genotype differences in exploratory behavior and retention memory (Supplementary Figure 1G-I). A main effect for genotype was observed for distance travelled ($F(2.36)= 12.90$, $p<0.0001$) and average speed ($F(2.36)= 12.72$, $p<0.0001$) in female mice. Female $APP^{NL-F/NL-F}$ mice showed significantly increased distance travelled and average speed compared to age-matched $APP^{NL/NL}$ ($p<0.0001$; $p=<0.0001$) and C57BL/6 mice ($p=0.0066$; $p=0.0068$), respectively, that was only exhibited during the retention day. No genotype differences were observed in retention memory for female mice. These findings indicate elevated exploratory behavior in female $APP^{NL-F/NL-F}$ mice during cognitive testing in agreement with previous studies (Kundu *et al.* 2021).

To characterize possible changes in hippocampal glutamate dynamics before cognitive decline, *in vivo* glutamate recordings were conducted on anesthetized mice following completion of the behavioral assays. For male mice, representative traces are shown in Figure 1A. No significant differences were observed in basal glutamate levels for any hippocampal subregion (Figure 1B). However, stimulation of surrounding neurons with 70mM KCl yielded a significant main effect for evoked glutamate release in the DG ($F(2,29)= 11.01$, $p=0.003$) and CA3 ($F(2,26)= 6.920$, $p=0.0039$) for male mice (Figure 1C). $APP^{NL-F/NL-F}$ male mice showed elevated stimulus-evoked glutamate release compared to age-matched $APP^{NL/NL}$ ($p=0.0016$, $p=0.0128$) and C57BL/6 mice ($p=0.0008$, $p= 0.0087$) in the DG and CA3. Time to 80% signal decay (T_{80}) was used to characterize glutamate clearance after stimulation, an important factor for maintaining glutamatergic homeostasis (Rudy *et al.* 2015; Revett *et al.* 2013; Valladolid-Acebes *et al.* 2012). Examination of T_{80} glutamate clearance indicated no significant differences for

male mice in any hippocampal subregion. These findings demonstrate early hyperactivation of glutamatergic neurotransmission prior to the onset of cognitive symptoms in male $APP^{NL-F/NL-F}$ mice.

Representative traces for young female mice are shown in Figure 2A. No significant differences in basal glutamate levels or stimulus-evoked glutamate release for any hippocampal subregion were observed (Figure 2B-C). Analysis of glutamate signal decay time yielded a significant main effect in the CA1 alone for female mice ($F(2,28)= 4.577$, $p=0.0191$) (Figure 2D). $APP^{NL-F/NL-F}$ females exhibited faster T_{80} clearance of glutamate compared to age-matched $APP^{NL/NL}$ ($p=0.0324$) and C57BL/6 mice ($p=0.0390$). Data support potentially altered glutamate clearance in the CA1 of young female $APP^{NL-F/NL-F}$ mice that may act as an early compensatory mechanism to prevent hyperactivity.

Aged AD mice exhibit sex-dependent selective cognitive decline

Previous literature indicates progressive cognitive decline in $APP^{NL-F/NL-F}$ mice, with modest deficits in spatial reversal learning and place preference learning observed at 13-17 months (Masuda *et al.* 2016) and spatial working memory at 18 months (Saito *et al.* 2014). At 18+ months old, no significant differences were observed for male mice during the learning trials (Figure 3A). A main effect for genotype was observed with cumulative distance from the platform ($F(2, 38)= 9.828$, $p= 0.0004$) and area under the curve (AUC) ($F(2,38)= 9.322$, $p=0.0005$) in female mice (Figure 3B). AUC for the five trial days was significantly elevated for female $APP^{NL-F/NL-F}$ mice compared to age-matched $APP^{NL/NL}$ ($p=0.0331$) and C57BL/6 mice ($p=0.0003$). Overall, female $APP^{NL-F/NL-F}$ mice had a slower spatial learning curve compared to age-matched C57BL/6 mice.

By the final training session, all mice had learned the location of the hidden escape platform. During the probe challenge that is used to evaluate long-term memory recall, a significant main effect was observed for cumulative distance from the platform in female mice ($F(2,38)= 7.716$, $p=0.0015$). Female $APP^{NL-F/NL-F}$ mice exhibited increased cumulative distance compared to age-matched $APP^{NL/NL}$ ($p= 0.0064$) and C57BL/6 mice ($p=0.0029$) (Figure 3C). No significant differences in cumulative distance were observed for male mice. However, analysis of platform entries per distance swam indicated a significant main effect for male mice ($F(2,38)= 5.978$, $p=0.0055$). $APP^{NL-F/NL-F}$ ($p=0.0043$) male mice showed a significant decrease in number of platform entries compared to age-matched C57BL/6 mice (Figure 3D). No significant genotype differences were observed for female mice on platform entries. Path efficiency to first platform entry was also examined and yielded no significant findings for either sex (Figure 3E). Representative path traces are shown in Figure 3F. These findings indicate sex differences in spatial learning and memory impairment with age in $APP^{NL-F/NL-F}$ mice, in agreement with prior aging literature examining this mouse model (Britz *et al.* 2022).

Data from the NOR task indicated no significant genotype differences on any parameters during the retention day for male mice (Figure 3G-I). Significant main effects were observed for distance ($F(2,37)= 3.947$, $p= 0.0279$), average speed ($F(2,37)= 4.006$, $p= 0.0266$), and novelty preference ($F(2,37)= 3.108$, $p= 0.0565$) in female mice. Female $APP^{NL/NL}$ female mice alone exhibited decreased distance ($p= 0.0310$) and average speed ($p= 0.0266$) compared to age-matched C57BL/6 mice (Figure 3G-H). $APP^{NL-F/NL-F}$ female mice showed significantly decreased novelty preference compared to age-matched C57BL/6 mice ($p=0.0453$) (Figure 3I). Together, data support impaired

spatial cognition and selective impairment of recognition memory in aged female $APP^{NL-F/NL-F}$ mice, indicating a potentially more severe cognitive phenotype for aged females than males in the $APP^{NL-F/NL-F}$ mouse model.

Temporal-specific alterations to hippocampal glutamate dynamics in aged AD mice

In vivo glutamate recordings were also conducted in aged mice to investigate possible changes in hippocampal glutamate dynamics with age and disease progression. Representative traces for aged male mice are shown in Figure 4A. Analysis of basal glutamate indicated a significant main effect in the CA3 ($F(2, 27)= 6.486$, $p=0.0050$) and the CA1 ($F(2, 25)= 3.437$, $p=0.0480$) for male mice (Figure 4B). $APP^{NL-F/NL-F}$ male mice exhibited decreased basal glutamate levels in the CA3 ($p=0.0193$) and the CA1 ($p= 0.0488$) compared to age-matched C57BL/6 male mice. No significant differences in basal glutamate were observed for $APP^{NL/NL}$ mice in any hippocampal subregion. A significant main effect for evoked glutamate release was observed in the DG ($F(2, 27)= 12.06$, $p=0.0002$) and CA3 ($F(2, 28)= 5.313$, $p=0.0111$) for male mice (Figure 4C). $APP^{NL/NL}$ ($p=0.0006$, $p=0.0209$) and $APP^{NL-F/NL-F}$ ($p=0.0009$, $p=0.0280$) male mice showed decreased stimulus-evoked glutamate release in the DG and CA3 compared to age-matched C57BL/6 mice. Analysis of T_{80} also indicated a significant main effect in the DG for aged male mice ($F(2, 27)= 3.579$, $p= 0.0418$). $APP^{NL/NL}$ male mice showed increased clearance time compared to C57BL/6 male mice ($p= 0.0333$; Figure 4D). These findings indicate a potentially subregion-specific hypoglutamatergic environment in the hippocampus of aged male AD mice and effectively demonstrate the hyper-to-

hypoactivation phenomenon for glutamatergic neurotransmission throughout disease progression in $APP^{NL-F/NL-F}$ male mice.

Representative traces for aged female mice are shown in Figure 5A. A significant main effect ($F(2, 29)= 5.080$, $p=0.0128$) was observed for basal glutamate levels in the CA1 alone for female mice (Figure 5B). Female $APP^{NL-F/NL-F}$ mice displayed decreased CA1 basal glutamate compared to age-matched C57BL/6 mice ($p=0.0093$). No differences in basal glutamate were observed for $APP^{NL/NL}$ female mice in any hippocampal subregion. Data support no significant differences in stimulus-evoked glutamate release in any subregion for aged female mice (Figure 5C). A main effect for T_{80} was observed in the DG for female mice ($F(2, 27)= 3.579$, $p=0.0418$). $APP^{NL/NL}$ female mice alone exhibited faster T_{80} than age-matched C57BL/6 mice ($p=0.0333$) (Figure 5D). Together, data support potential alterations in glutamate clearance and regulation of the glutamatergic homeostasis with age in female $APP^{NL-F/NL-F}$ mice and a unique biological aging process from that observed in male $APP^{NL-F/NL-F}$ mice.

Discussion

This study aimed to characterize glutamatergic neurotransmission throughout disease progression in the $APP^{NL-F/NL-F}$ mouse model of AD. We utilized a glutamate biosensor to record hippocampal glutamatergic neurotransmission *in vivo* in both sexes at young (2-4 months old) and aged (18+ months old) time points to address this question. Further, we implemented the use of multiple sex- and age-matched C57BL/6 groups, including the $APP^{NL/NL}$ model, to eliminate confounding variables and better analyze the role of $A\beta_{42}$ pathology. We hypothesized that $APP^{NL-F/NL-F}$ mice would exhibit presymptomatic hippocampal glutamatergic hyperactivation that shifts with age and

disease progression. Our findings indicated a more severe cognitive phenotype in aged female $APP^{NL\text{-}F/NL\text{-}F}$ mice than genotype- and age-matched males, and demonstrated sex differences in hippocampal glutamate dynamics throughout the lifespan. These outcomes reflect that of human AD pathology, in which females bear a heavier disease burden and distinct cognitive profile (Alzheimer's Association 2022; Podcasy and Epperson 2016; Laws *et al.* 2016).

Hippocampal glutamate recordings demonstrated a hyper-to-hypoactivation event for glutamatergic neurotransmission throughout the lifespan of $APP^{NL\text{-}F/NL\text{-}F}$ male mice. Before the onset of cognitive symptoms, young male $APP^{NL\text{-}F/NL\text{-}F}$ mice displayed increased evoked glutamate release in the DG and CA3 hippocampal subregions. These were the same subregions in which we observed depleted evoked glutamate release in aged $APP^{NL\text{-}F/NL\text{-}F}$ male mice. A decrease in basal glutamate in the CA1 and CA3 subregions was also observed in these mice, supporting a hypoactive glutamatergic environment with age and disease progression. Loss of glutamatergic stimulation of postsynaptic receptors would impair hippocampal long-term potentiation and confer impaired performance on memory tasks (Findley *et al.* 2019; Hascup *et al.* 2020; Parsons *et al.* 2007). Soluble $A\beta_{42}$ appears as a likely driver of hyper-to-hypoactivation, as early hyperactivation was not observed in young male $APP^{NL/NL}$ mice that only express increased total amyloid levels and not specific preference for $A\beta_{42}$ production. Soluble $A\beta_{42}$ has been shown to directly interact with the glutamatergic synapse and drive dyshomeostasis with disease progression (Findley *et al.* 2019; Hascup *et al.* 2022; Hascup and Hascup 2016; Ferreira and Klein 2011; Wilcox *et al.* 2011). Further, elevated soluble $A\beta_{42}$ has been characterized in male $APP^{NL\text{-}F/NL\text{-}F}$ mice

beginning around 2 months of age, concurrent with the window of hyperactivation observed in this study (Saito *et al.* 2014; Masuda *et al.* 2016). However, aged male $APP^{NL/NL}$ mice showed decreased evoked glutamate release in the same subregions as age-matched $APP^{NL-F/NL-F}$ mice, leaving open the possibility of multiple drivers for glutamatergic hypoactivation in later disease stages.

Data from glutamate recordings in male $APP^{NL-F/NL-F}$ mice varies from that previously obtained by our laboratory in transgenic AβPP/PS1 male mice (Hascup *et al.* 2020). Namely, we observed a steady incline in basal glutamate levels in all subregions of the hippocampus in AβPP/PS1 male mice that was absent in male $APP^{NL-F/NL-F}$ mice— and juxtaposed for the CA3 and CA1 with age and disease progression. Further, a similar hyper-to-hypoactivation event occurred with disease progression in male AβPP/PS1 mice, but primarily in the CA1 instead of the DG and CA3 as observed in $APP^{NL-F/NL-F}$ male mice. This divergence could be due to differences between the mouse models including gene overexpression and transgenic versus knock-in genetic manipulation. AβPP/PS1 exhibit greater amyloid burden, higher early attrition rate, and more aggressive cognitive decline (Britz *et al.* 2022). However, previous studies have shown a similar amyloidosis timeline between AβPP/PS1 and $APP^{NL-F/NL-F}$ mice, first appearing in cortex and hippocampus (Saito *et al.* 2014; Masuda *et al.* 2016; Hascup *et al.* 2020; Britz *et al.* 2022). Temporal progression through the hippocampus is also similar between the models, occurring first and primarily in the CA1 and then moving into the DG and CA3 (Britz *et al.* 2022; Hascup *et al.* 2020). Yet, the temporal progression for amyloidosis and glutamate hyperactivity in male AβPP/PS1 mice mirror each other, unlike that observed in $APP^{NL-F/NL-F}$ mice. Other intermediating factors may come into

play – such as mouse model differences in the expression of key glutamate synaptic components across hippocampal subregions – and should be explored in future studies.

Female $APP^{NL-F/NL-F}$ mice underwent a unique and divergent biological aging process to that characterized in male $APP^{NL-F/NL-F}$ mice. No alterations in evoked glutamate release appeared throughout the lifespan for $APP^{NL-F/NL-F}$ female mice — their story pertained more to glutamate clearance and homeostatic maintenance. Young $APP^{NL-F/NL-F}$ female mice showed faster glutamate clearance times compared to age-matched $APP^{NL/NL}$ and C57BL/6 mice in the CA1. The same subregion then showed a loss of basal glutamate levels in aged female $APP^{NL-F/NL-F}$ mice, indicating a possible early compensatory mechanism to maintain glutamatergic homeostasis that failed with disease progression. Glutamatergic transport is the crux of homeostasis at the tripartite glutamate synapse — dysregulation of astrocytic glutamate clearance can significantly impact cognitive outcomes (Varga *et al.* 2015; Lewerenz and Maher 2015b; Sheldon and Robinson 2007). Of note, a prior study from our laboratory found that local $A\beta_{42}$ application stimulated lactate release only in the CA1 of female C57BL/6 mice, a possible indication of $A\beta_{42}$-mediated increased glutamate clearance localized to this hippocampal subregion in female mice (Hascup *et al.* 2022). It is possible that glutamatergic alterations exist more in tonic or spontaneous activity for $APP^{NL-F/NL-F}$ female mice than with stimulus-evoked glutamate release. Such a possibility would explain the absence of effects to evoked glutamate release, and provide more context to faster glutamate clearance times in young $APP^{NL-F/NL-F}$ female mice. Another possible explanation may reside in astrocyte activity and response to pathology, in which prior studies indicate sexual dimorphism and emphasize the neuromodulatory role of estrogen (Chowen and

Garcia-Segura 2021). Estrogen can protect against glutamate hyperexcitability by supporting astrocyte function and inhibitory regulation (Spencer *et al.* 2008; Nematipour *et al.* 2020) — and yield devastating biological consequences when lost during menopause (Wang *et al.* 2020; Georgakis *et al.* 2019). Taken together, there are likely multiple factors contributing to the difference in hippocampal glutamate dynamics with disease progression for female $APP^{NL\text{-}F/NL\text{-}F}$ mice.

Glutamate findings in female $APP^{NL\text{-}F/NL\text{-}F}$ mice contrast that of previous studies from other laboratories in female AβPP/PS1 mice (Minkeviciene *et al.* 2008). A loss of hippocampal evoked glutamate response with disease progression was reported, with no alterations to basal glutamate throughout the lifespan. Prior examination of amyloid pathology from both models indicate more aggressive amyloidosis in female AβPP/PS1 mice, with both models following a similar temporal progression observed in their male counterparts (Britz *et al.* 2022). At 12 months of age, female AβPP/PS1 mice display more severe amyloid pathology, especially in the hippocampus, than male AβPP/PS1 mice (Jiao *et al.* 2016). It is possible that the severity of amyloid pathology observed in female AβPP/PS1 mice drove the glutamatergic hypoactivity observed in later disease stages and would explain the absence of this effect in $APP^{NL\text{-}F/NL\text{-}F}$ female mice.

Further considerations should also be given to the role of estrogen between these models. Female C57BL/6 mice — and AD mice on a C57BL/6 background — reach reproductive senescence and become acyclic between 12-16 months of age (Holinka *et al.* 1979; Mobbs *et al.* 1984; Clinton *et al.* 2007). Studies have found that aging reduces the neuroprotective action of 17β-estradiol treatment in transgenic AD mice (Christensen *et al.* 2020). To that end, data support that 17β-estradiol replacement in

ovariectomized female AβPP/PS1 mice only exerts procognitive effects in early stages (4 months of age) (Qin *et al.* 2020). AβPP/PS1 female mice also display an increased pro-inflammatory profile and greater neuronal and synaptic degeneration than that of their male counterparts, which may be driven in-part by loss of responsiveness to estrogen (Jiao *et al.* 2016). It remains uncertain whether $APP^{NL\text{-}F/NL\text{-}F}$ female mice display similar deficiencies, which would impact both the glutamate and cognitive outcomes observed in this study (Luo *et al.* 2022; Barth *et al.* 2015; Nematipour *et al.* 2020).

Results from our behavioral analysis indicated sexual dimorphism in cognitive deficits for $APP^{NL\text{-}F/NL\text{-}F}$ aged mice. Aged male $APP^{NL\text{-}F/NL\text{-}F}$ mice exhibited impaired spatial long-term memory during the MWM, but did not show any loss in recognition memory. These findings are congruent with previous studies examining cognition in $APP^{NL\text{-}F/NL\text{-}F}$ mice (Masuda *et al.* 2016; Saito *et al.* 2014; Britz *et al.* 2022; Mazzei *et al.* 2021). Aged $APP^{NL/NL}$ male mice did not exhibit deficits in spatial or retention memory, in agreement with previous studies examining 24-month-old male $APP^{NL/NL}$ mice (Salas *et al.* 2018). It is possible that prolonged glutamatergic dyshomeostasis in multiple subregions for $APP^{NL\text{-}F/NL\text{-}F}$ male mice contributed to an earlier onset of cognitive symptoms than $APP^{NL/NL}$ mice. Aged female $APP^{NL\text{-}F/NL\text{-}F}$ mice showed impaired spatial learning and memory and recognition memory, collectively displaying a more severe cognitive phenotype than that observed in male mice. As previously discussed, this may be due to loss of astrocytic homeostatic regulation of the glutamatergic synapse with disease progression. This finding mirrors previous studies indicating that AD tends to be more aggressive in female AD mice and in humans (Mielke 2018; Jiao *et al.* 2016). Spatial

long-term memory impairment for female $APP^{NL-F/NL-F}$ mice was also observed on a different parameter than genotype- and age-matched male mice during the MWM probe challenge. It is possible that sex differences in spatial navigation and wayfinding could have impacted the parameters by which cognitive deficits were observed (Andreano and Cahill 2009). Previous studies would indicate that this divergence between sexes is unlikely to be attributed to sex differences in executive function (Grissom and Reyes 2019). Sexual dimorphism in glutamate and cognition have been previously described (Giacometti and Barker 2020; Barth *et al.* 2015; Hädel *et al.* 2013), and support that differences in hippocampal glutamate dynamics observed throughout the lifespan may have also influenced sex differences in cognitive decline for this model.

Collectively, these findings indicate genotype and sex differences in glutamate dynamics and cognition for knock-in AD mice. $APP^{NL/NL}$ mice provided a necessary middle ground between C57BL/6 littermates and $APP^{NL-F/NL-F}$ mice to delineate the role of $A\beta_{42}$ in study outcomes. Further, these genotype differences also support that APP knock-in alone exerts moderate pathology, which is compounded by increased $A\beta_{42}$ production generating a more severe cognitive profile. Biological differences in sex add on another layer of complexity to the observed findings and point to worsened pathology in female mice likely implicating a hormonal impact to glutamate and cognition with age and disease progression that warrants further study.

Sexually dimorphic rates of biological aging may also contribute to the differences in glutamate dynamics and cognitive performance. Evidence suggests females maintain better cellular health for most of their life, but become frailer when approaching older age than males (Hägg and Jylhävä 2021). Divergent disease progression between the

sexes would hold important implications for therapeutic treatment. Interventional strategies must evaluate opportune windows for treatment that are tailored to the sex-specific degeneration timelines and broader disease pathogenesis to maximize efficacy. Further, these findings also reinforce that experimentation protocols for therapeutic candidates need to include evaluations of male and female participants. It is entirely plausible that intervention strategies may produce variable outcomes between sexes due to hormonal neuromodulation and sex-dependent pathogenic phenotype.

Author Contribution

CAF executed electrochemistry recordings, behavioral assays, data analysis and interpretation, and drafting of the manuscript. SAM assisted with conducting behavioral assays.TH assisted with cryosectioning and cresyl violet staining. MRP and KQ managed the breeding colony. KNH and ERH conceived and supervised the study, imparted surgical and electrochemistry training, , and provided manuscript revisions.

Acknowledgements

The authors have no acknowledgments to report.

References

Alzheimer's Association (2022) 2022 Alzheimer's disease facts and figures. **18**, 700–789.

Andreano J. M., Cahill L. (2009) Sex influences on the neurobiology of learning and memory. *Learn. Mem.* **16**, 248–266.

Barth C., Villringer A., Sacher J. (2015) *Sex hormones affect neurotransmitters and shape the adult female brain during hormonal transition periods*. Frontiers Research Foundation.

Britz J., Ojo E., Dhukhwa A., Saito T., Saido T. C., Hascup E. R., Hascup K. N., Tischkau S. A. (2022) Assessing Sex-Specific Circadian, Metabolic, and Cognitive Phenotypes in the AβPP/PS1 and APPNL-F/NL-F Models of Alzheimer's Disease. *J. Alzheimer's Dis.* **85**, 1077–1093.

Chowen J. A., Garcia-Segura L. M. (2021) Role of glial cells in the generation of sex differences in neurodegenerative diseases and brain aging. *Mech. Ageing Dev.* **196**, 111473.

Christensen A., Liu J., Pike C. J. (2020) Aging Reduces Estradiol Protection Against Neural but Not Metabolic Effects of Obesity in Female 3xTg-AD Mice. *Front. Aging Neurosci.* **12**, 113.

Clinton L. K., Billings L. M., Green K. N., Caccamo A., Ngo J., Oddo S., McGaugh J. L., LaFerla F. M. (2007) Age-dependent sexual dimorphism in cognition and stress response in the 3xTg-AD mice. *Neurobiol. Dis.* **28**, 76–82.

Cox M. F., Hascup E. R., Bartke A., Hascup K. N. (2022) Friend or Foe? Defining the Role of Glutamate in Aging and Alzheimer's Disease. *Front. Aging* **3**, 65.

Ferreira S. T., Klein W. L. (2011) The Aβ oligomer hypothesis for synapse failure and memory loss in Alzheimer's disease. *Neurobiol. Learn. Mem.* **96**, 529–543.

Findley C. A. C. A., Bartke A., Hascup K. N. K. N., Hascup E. R. E. R. (2019) Amyloid Beta-Related Alterations to Glutamate Signaling Dynamics During Alzheimer's Disease Progression. *ASN Neuro* **11**, 1–20.

Gasiorowska A., Wydrych M., Drapich P., Zadrozny M., Steczkowska M., Niewiadomski W., Niewiadomska G. (2021) *The Biology and Pathobiology of Glutamatergic, Cholinergic, and Dopaminergic Signaling in the Aging Brain*. Frontiers Media S.A.

Georgakis M. K., Beskou-Kontou T., Theodoridis I., Skalkidou A., Petridou E. T. (2019) Surgical menopause in association with cognitive function and risk of dementia: A systematic review and meta-analysis. *Psychoneuroendocrinology* **106**, 9–19.

Giacometti L. L., Barker J. M. (2020) *Sex differences in the glutamate system: Implications for addiction*. Elsevier Ltd.

Grissom N. M., Reyes T. M. (2019) *Let's call the whole thing off: evaluating gender and sex differences in executive function*. Nature Publishing Group.

Hädel S., Wirth C., Rapp M., Gallinat J., Schubert F. (2013) Effects of age and sex on the concentrations of glutamate and glutamine in the human brain. *J. Magn. Reson. Imaging* **38**, 1480–1487.

Hägg S., Jylhävä J. (2021) Sex differences in biological aging with a focus on human studies. *Elife* **10**.

Hascup E. R., Sime L. N., Peck M. R., Hascup K. N. (2022) Amyloid-β42 stimulated hippocampal lactate release is coupled to glutamate uptake. *Sci. Reports 2022 121* **12**, 1–11.

Hascup K. N., Findley C. A., Sime L. N., Hascup E. R. (2020) Hippocampal alterations in glutamatergic signaling during amyloid progression in AβPP/PS1 mice. *Sci. Rep.* **10**, 14503.

Hascup K. N., Hascup E. R. (2015) Altered neurotransmission prior to cognitive decline in AβPP/PS1 mice, a model of Alzheimer's disease. *J. Alzheimer's Dis.* **44**, 771–776.

Hascup K. N., Hascup E. R. (2016) Soluble Amyloid-β42 Stimulates Glutamate Release through Activation of the α7 Nicotinic Acetylcholine Receptor. *J. Alzheimer's Dis.* **53**, 337–347.

Hascup K. N., Rutherford E. C., Quintero J. E., Day B. K., Nickell J. R., Pomerleau F., Huettl P., Burmeister J. J., Gerhardt G. A. (2007) Second-by-Second Measures of L-Glutamate and Other Neurotransmitters Using Enzyme-Based Microelectrode Arrays, in *Electrochem. Methods Neurosci.* CRC Press/Taylor & Francis.

Holinka C. F., Tseng Y.-C., Finch C. E. (1979) Reproductive Aging in C57BL/6J Mice: Plasma Progesterone, Viable Embryos and Resorption Frequency throughout Pregnancy1. *Biol. Reprod.* **20**, 1201–1211.

Jiao S. S., Bu X. Le, Liu Y. H., Zhu C., Wang Q. H., Shen L. L., Liu C. H., Wang Y. R., Yao X. Q., Wang Y. J. (2016) Sex Dimorphism Profile of Alzheimer's Disease-Type Pathologies in an APP/PS1 Mouse Model. *Neurotox. Res.* **29**, 256–266.

Kundu P., Torres E. R. S., Stagaman K., Kasschau K., Okhovat M., Holden S., Ward S., Nevonen K. A., Davis B. A., Saito T., Saido T. C., Carbone L., Sharpton T. J., Raber J. (2021) Integrated analysis of behavioral, epigenetic, and gut microbiome analyses in App NL-G-F, App NL-F, and wild type mice. *Sci. Rep.* **11**, 4678.

Laws K. R., Irvine K., Gale T. M. (2016) Sex differences in cognitive impairment in Alzheimer's disease. *World J. Psychiatry* **6**, 54.

Lewerenz J., Maher P. (2015a) *Chronic glutamate toxicity in neurodegenerative diseases-What is the evidence?* Frontiers Media S.A.

Lewerenz J., Maher P. (2015b) *Chronic glutamate toxicity in neurodegenerative diseases-What is the evidence?* Frontiers Media S.A.

Luo M., Zeng Q., Jiang K., Zhao Y., Long Z., Du Y., Wang K., He G. (2022) Estrogen deficiency exacerbates learning and memory deficits associated with glucose

563 metabolism disorder in APP/PS1 double transgenic female mice. *Genes Dis.* **9**,
564 1315–1331.

565 Masuda A., Kobayashi Y., Kogo N., Saito T., Saido T. C., Itohara S. (2016) Cognitive
566 deficits in single App knock-in mouse models. *Neurobiol. Learn. Mem.* **135**, 73–82.

567 Mazzei G., Ikegami R., Abolhassani N., Haruyama N., Sakumi K., Saito T., Saido T. C.,
568 Nakabeppu Y. (2021) A high-fat diet exacerbates the Alzheimer's disease
569 pathology in the hippocampus of the App NL−F/NL−F knock-in mouse model.
570 *Aging Cell* **20**, e13429.

571 McEntee W. J., Crook T. H. (1993) *Glutamate: its role in learning, memory, and the*
572 *aging brain*. Springer-Verlag.

573 Mielke M. M. (2018) Sex and gender differences in Alzheimer disease dementia.
574 *Psychiatr. Times* **35**, 14–15.

575 Minkeviciene R., Ihalainen J., Malm T., Matilainen O., Keksa-Goldsteine V., Goldsteins
576 G., Iivonen H., Leguit N., Glennon J., Koistinaho J., Banerjee P., Tanila H. (2008)
577 Age-related decrease in stimulated glutamate release and vesicular glutamate
578 transporters in APP/PS1 transgenic and wild-type mice. *J. Neurochem.* **105**, 584–
579 594.

580 Mobbs C. V., Gee D. M., Finch C. E. (1984) Reproductive senescence in female
581 C57BL/6J mice: Ovarian impairments and neuroendocrine impairments that are
582 partially reversible and delayable by ovariectomy. *Endocrinology* **115**, 1653–1662.

583 Nematipour S., Vahidinia Z., Nejati M., Naderian H., Beyer C., Tameh A. A. (2020)
584 Estrogen and progesterone attenuate glutamate neurotoxicity via regulation of
585 EAAT3 and GLT-1 in a rat model of ischemic stroke. *Iran. J. Basic Med. Sci.* **23**,
586 1346–1352.

587 Olney J. W., Wozniak D. F., Farber N. B. (1997) Excitotoxic neurodegeneration in
588 Alzheimer disease. New hypothesis and new therapeutic strategies. *Arch. Neurol.*
589 **54**, 1234–40.

590 Parsons C. G., Stöffler A., Danysz W. (2007) Memantine: a NMDA receptor antagonist
591 that improves memory by restoration of homeostasis in the glutamatergic system -
592 too little activation is bad, too much is even worse. *Neuropharmacology* **53**, 699–
593 723.

594 Podcasy J. L., Epperson C. N. (2016) Considering sex and gender in Alzheimer disease
595 and other dementias. *Dialogues Clin. Neurosci.* **18**, 437–446.

596 Purves D, Augustine GJ, Fitzpatrick D (2001) Glutamate, in *Neuroscience*. Sinauer
597 Associates, Sunderland (MA).

598 Qin Y., An D., Xu W., Qi X., Wang X., Chen L., Chen L., Sha S. (2020) Estradiol
599 Replacement at the Critical Period Protects Hippocampal Neural Stem Cells to
600 Improve Cognition in APP/PS1 Mice. *Front. Aging Neurosci.* **12**, 240.

601 Revett T. J., Baker G. B., Jhamandas J., Kar S. (2013) Glutamate system, amyloid ß

peptides and tau protein: functional interrelationships and relevance to Alzheimer disease pathology. *J. Psychiatry Neurosci.* **38**, 6–23.

Rudy C. C., Hunsberger H. C., Weitzner D. S., Reed M. N. (2015) The Role of the Tripartite Glutamatergic Synapse in the Pathophysiology of Alzheimer's Disease. *Aging Dis.* **6**, 131–148.

Saito T., Matsuba Y., Mihira N., Takano J., Nilsson P., Itohara S., Iwata N., Saido T. C. (2014) Single App knock-in mouse models of Alzheimer's disease. *Nat. Neurosci.* **17**, 661–663.

Salas I. H., Callaerts-Vegh Z., D'Hooge R., Saido T. C., Dotti C. G., Strooper B. De, D'Hooge R., Saido T. C., Dotti C. G., Strooper B. De (2018) Increased Insoluble Amyloid-β Induces Negligible Cognitive Deficits in Old APPNL/NL Knock-In Mice. **66**, 801–809.

Segovia G., Porras A., Arco A. Del, Mora F. (2001) Glutamatergic neurotransmission in aging: A critical perspective. *Mech. Ageing Dev.* **122**, 1–29.

Shah D., Latif-Hernandez A., Strooper B. De, Saito T., Saido T., Verhoye M., D'Hooge R., Linden A. Van der, D'Hooge R., Linden A. Van der (2018) Spatial reversal learning defect coincides with hypersynchronous telencephalic BOLD functional connectivity in APPNL-F/NL-F knock-in mice. **8**, 6264.

Sheldon A. L., Robinson M. B. (2007) *The role of glutamate transporters in neurodegenerative diseases and potential opportunities for intervention*. Elsevier Ltd.

Spencer J. L., Waters E. M., Romeo R. D., Wood G. E., Milner T. A., McEwen B. S. (2008) *Uncovering the mechanisms of estrogen effects on hippocampal function*. NIH Public Access.

Valladolid-Acebes I., Merino B., Principato A., Fole A., Barbas C., Lorenzo M. P., García A., Olmo N. Del, Ruiz-Gayo M., Cano V. (2012) High-fat diets induce changes in hippocampal glutamate metabolism and neurotransmission. *Am. J. Physiol. Metab.* **302**, E396–E402.

Varga E., Juhász G., Bozsó Z., Penke B., Fülöp L., Szegedi V. (2015) Amyloid-β1-42 Disrupts Synaptic Plasticity by Altering Glutamate Recycling at the Synapse. *J. Alzheimers. Dis.* **45**, 449–456.

Wang Y., Shang Y., Mishra A., Bacon E., Yin F., Brinton R. (2020) Midlife Chronological and Endocrinological Transitions in Brain Metabolism: System Biology Basis for Increased Alzheimer's Risk in Female Brain. *Sci. Rep.* **10**, 8528–8528.

Wilcox K. C., Lacor P. N., Pitt J., Klein W. L. (2011) Aβ Oligomer-Induced Synapse Degeneration in Alzheimer's Disease. *Cell. Mol. Neurobiol.* **31**, 939–948.

Figure Legend

Figure 1: *Elevated evoked glutamate release in 2-4 months old APP$^{NL-F/NL-F}$ male mice.* A) Representative traces of 70 mM KCl stimulus-evoked glutamate recordings in the DG, CA3, and CA1 hippocampal subregions. B-C) Basal and stimulus-evoked glutamate concentration by subregion. Inset depicts average amount of 70 mM KCl locally applied to evoke glutamate release. D) Time to 80% of glutamate clearance. One-way ANOVA, Tukey's post-hoc, *p<0.05, **p<0.01.

Figure 2: *Altered glutamate clearance in the CA1 of 2-4 months old female APP$^{NL-F/NL-F}$ mice.* A) Representative traces of 70 mM KCl stimulus-evoked glutamate recordings in the DG, CA3, and CA1 hippocampal subregions. B-C) Basal and stimulus-evoked glutamate concentration by subregion. Inset depicts average amount of 70 mM KCl locally applied to evoke glutamate release. D). Time to 80% of glutamate clearance. One-way ANOVA, Tukey's post-hoc, *p<0.05.

Figure 3: *Sex-dependent cognitive decline in aged AD mice.* A-B) Cumulative distance to the platform throughout the five trial days for male (A) and female (B) mice. Insets depict area under the curve (AUC) for the five-day learning period. C-E) Probe challenge measures include: cumulative distance, platform entries per distance swam, and path efficiency to first entry. F) Representative track plots from the probe challenge for each sex and genotype. G-H) Distance and average speed during the novel object retention day. I) Evaluation of retention memory through novelty preference. MWM Trials: Two-way ANOVA, Tukey's post-hoc; MWM Probe and NOR: One-way ANOVA, Tukey's post-hoc, *p<0.05, **p<0.01, ***p<0.001.

Figure 4: *Hypoactive glutamate dynamics in the hippocampus of 18+ months old male AD mice.* A) Representative traces from 70 mM KCl stimulus-evoked glutamate recordings in the DG, CA3, and CA1 hippocampal subregions. B-C) Basal and stimulus-evoked glutamate concentration by subregion. Inset depicts average amount of 70 mM KCl locally applied to evoke glutamate release. D) Time to 80% of glutamate clearance. One-way ANOVA, Tukey's post-hoc, *p<0.05, ***p<0.001.

Figure 5: *Decreased basal glutamate levels in the CA1 of 18+ months old female $APP^{NL\text{-}F/NL\text{-}F}$ mice.* A) Representative traces from the DG, CA3, and CA1. B-C) Basal and stimulus-evoked glutamate concentration by subregion. Inset depicts average amount of 70 mM KCl locally applied to evoke glutamate release. D) Time to 80% of glutamate clearance. One-way ANOVA, Tukey's post-hoc, *p<0.05, **p<0.01.

Supplementary Figure 1: *No memory deficits present in 2-4 months old knock-in AD mice.* A-B) Spatial learning performance evaluated by cumulative distance from the platform area throughout the five trial days for male (A) and female (B) mice. C-E) Long-term spatial memory recall performance during probe challenge was measured by: cumulative distance, platform entries per distance swam, and path efficiency to first entry. G-H) Distance and average speed during the novel object retention day. I) Evaluation of retention memory through novelty preference. MWM Trials: Two-way ANOVA, Tukey's post-hoc; MWM Probe and NOR: One-way ANOVA, Tukey's post-hoc, **p<0.01, ****p<0.0001

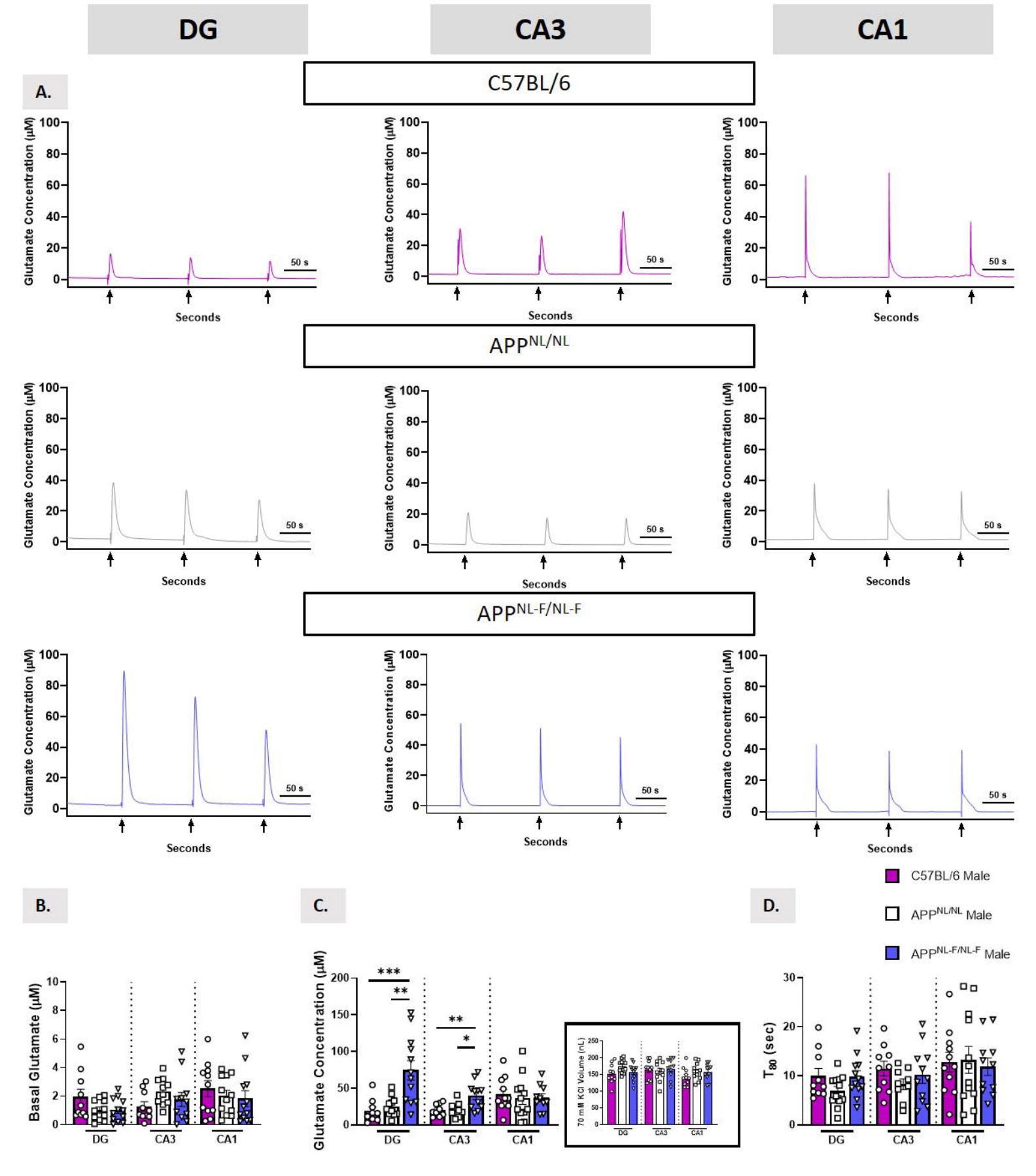
DG
CA3
CA1
A.
C57BL/6
APPNL/NL
APPNL-F/NL-F
Glutamate Concentration (μM)
Seconds
50 s
B.
Basal Glutamate (μM)
C.
Glutamate Concentration (μM)
70 mM KCl Volume (nL)
D.
T80 (sec)
C57BL/6 Male
APPNL/NL Male
APPNL-F/NL-F Male

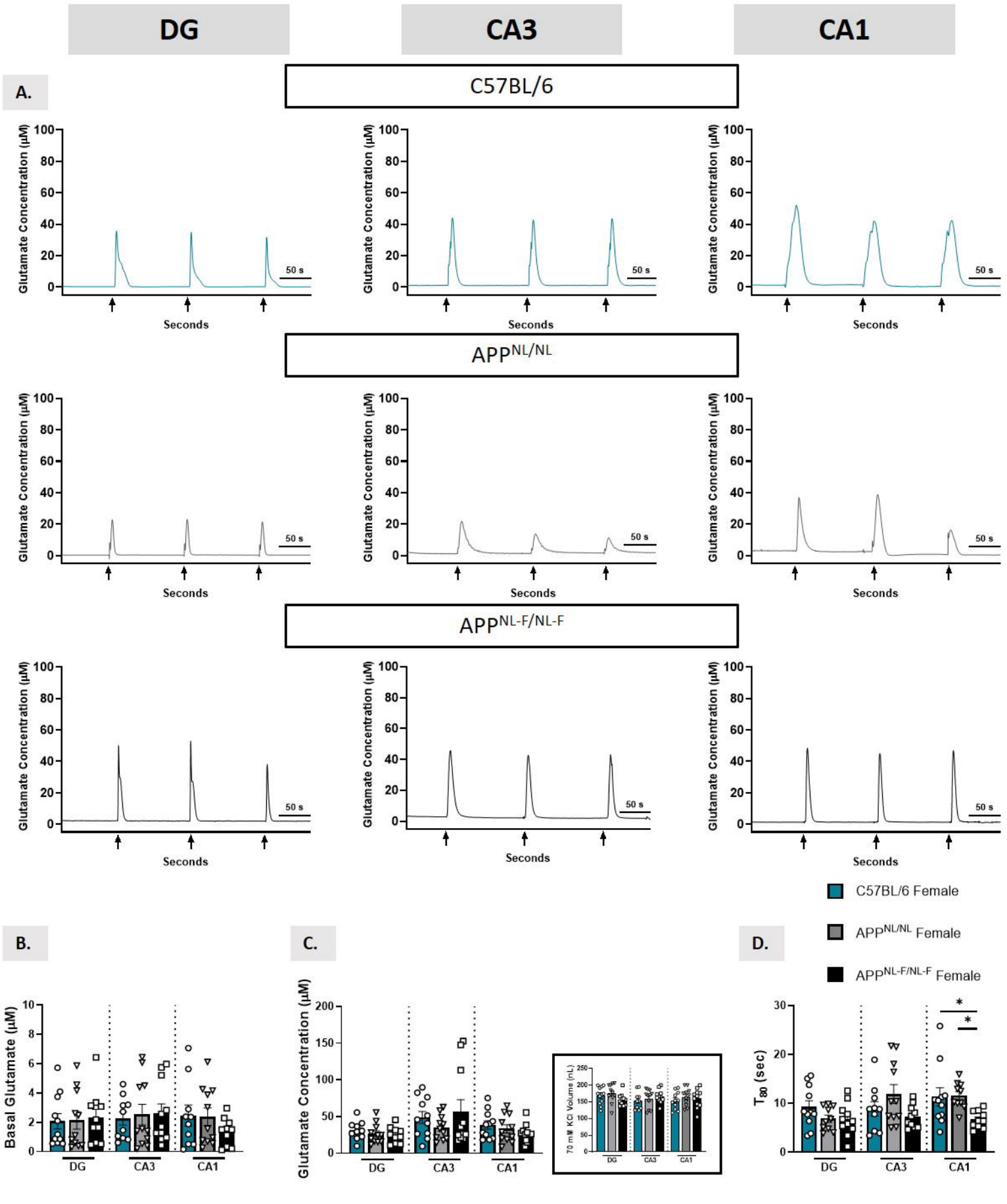
DG
CA3
CA1
A.
C57BL/6
APPNL/NL
APPNL-F/NL-F
Glutamate Concentration (μM)
Seconds
50 s
B.
Basal Glutamate (μM)
C.
Glutamate Concentration (μM)
70 mM KCl Volume (nL)
D.
T80 (sec)
C57BL/6 Female
APPNL/NL Female
APPNL-F/NL-F Female

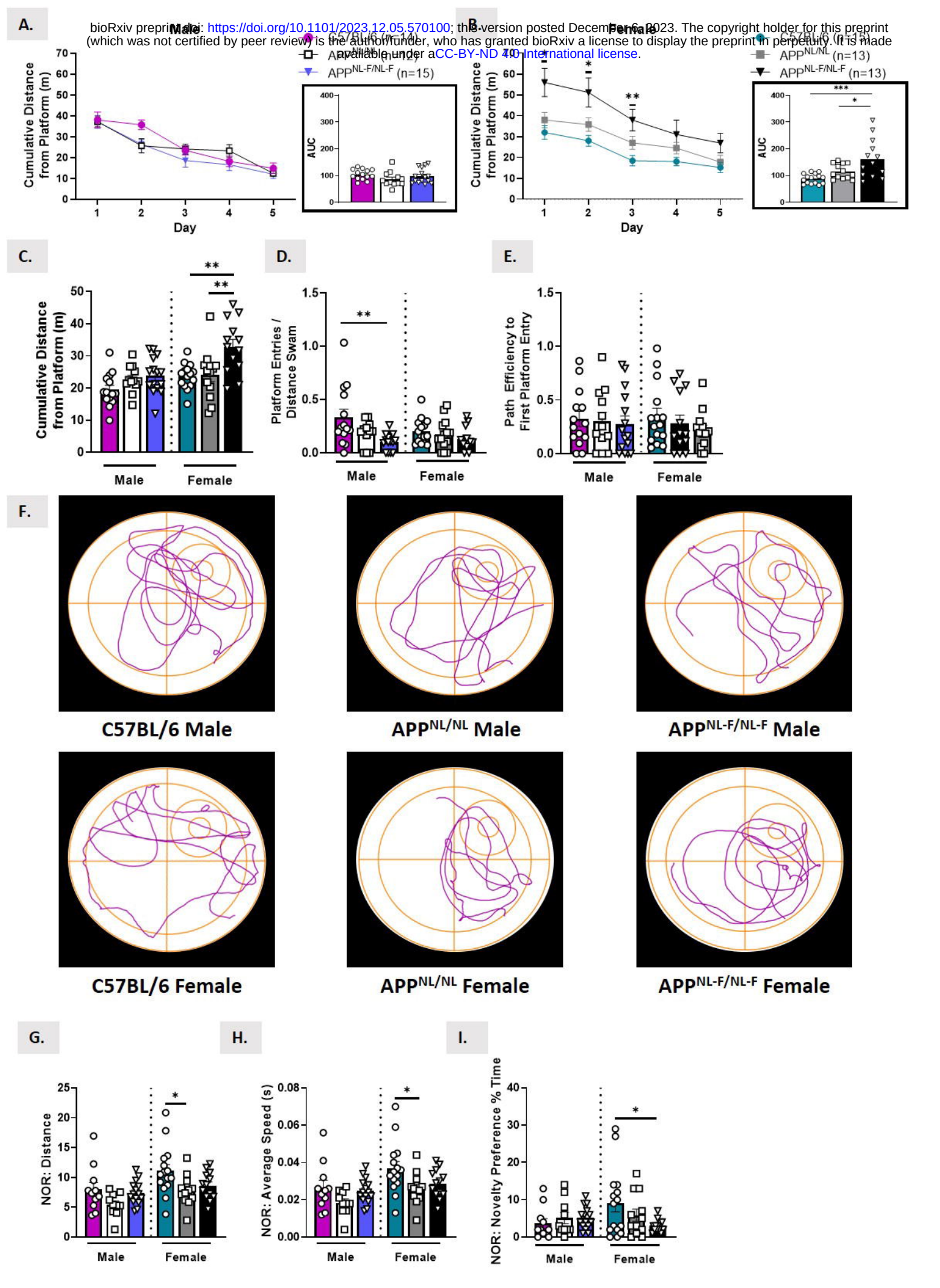

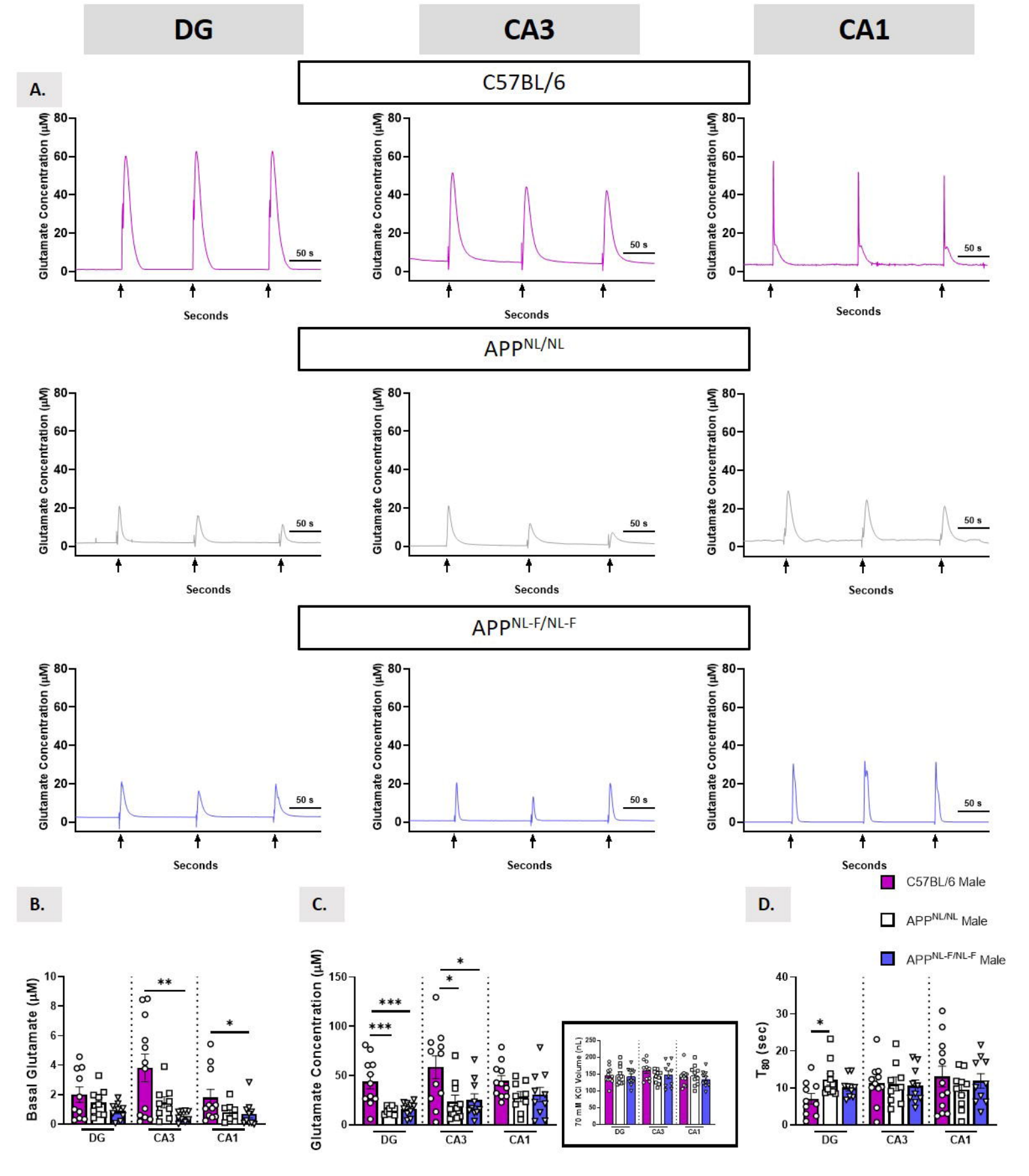
DG
CA3
CA1
A.
C57BL/6
APP^NL/NL
APP^NL-F/NL-F
Glutamate Concentration (μM)
Seconds
50 s
B.
Basal Glutamate (μM)
C.
Glutamate Concentration (μM)
70 mM KCl Volume (nL)
D.
T80 (sec)
C57BL/6 Male
APP^NL/NL Male
APP^NL-F/NL-F Male

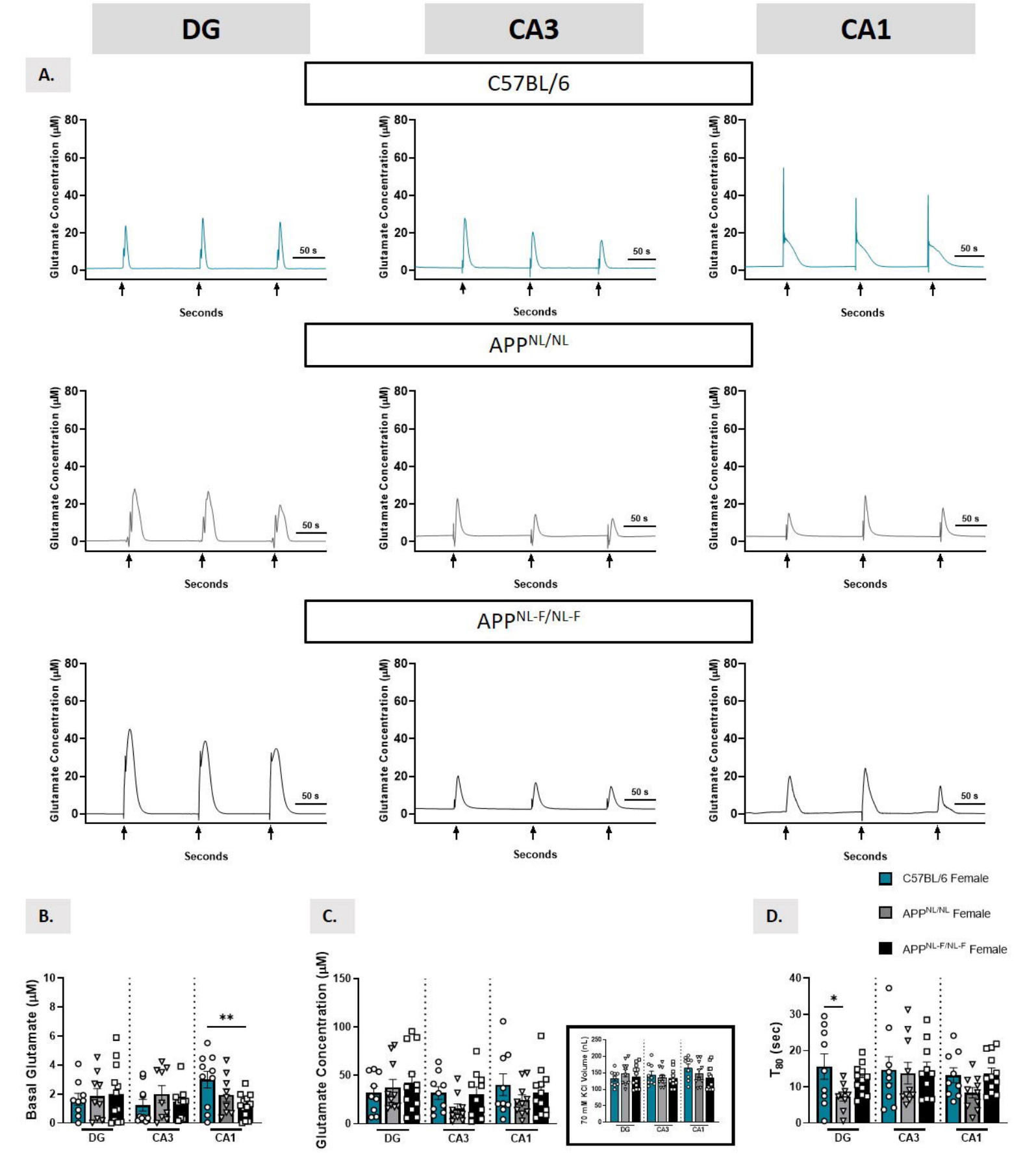
DG
CA3
CA1
A.
C57BL/6
APPNL/NL
APPNL-F/NL-F
Glutamate Concentration (μM)
Seconds
50 s
B.
Basal Glutamate (μM)
**
C.
Glutamate Concentration (μM)
70 mM KCl Volume (nL)
D.
T80 (sec)
*
C57BL/6 Female
APPNL/NL Female
APPNL-F/NL-F Female